PHYSICAL REVIEW C VOLUME 21, NUMBER 4 APRIL 1980

Giant resonance for the actinide nuclei: Photoneutron and photofission cross sections for ^{235}U, ^{236}U, ^{238}U, and ^{232}Th

J. T. Caldwell and E. J. Dowdy
Los Alamos Scientific Laboratory, University of California, Los Alamos, New Mexico 87545

B. L. Berman, R. A. Alvarez, and P. Meyer
Lawrence Livermore Laboratory, University of California, Livermore, California 94550

(Received 21 November 1979)

The photoneutron cross sections $\sigma(\gamma,n)$ and $\sigma(\gamma,2n)$, and total photofission cross sections $\sigma(\gamma,F)$ have been measured for ^{235}U, ^{236}U, ^{238}U, and ^{232}Th from threshold to 18.3 MeV using monoenergetic photons from the annihilation in flight of fast positrons and neutron-multiplicity detection in an efficient 4π neutron detector. Use of the ring-ratio technique allowed both the average photofission neutron energy for each nucleus to be obtained as a function of photon energy and, for ^{236}U and ^{238}U, the determination of the partial cross sections for first-chance $\sigma(\gamma,f)$ and second-chance $\sigma(\gamma,nf)$ photofission as well. Information extracted from the data includes integrated cross sections and their moments, giant-resonance parameters, deformation and radius parameters, and relative and absolute neutron and fission probabilities.

[NUCLEAR REACTIONS ^{235,236,238}U and ^{232}Th $(\gamma,n,2n,F)$, $E_\gamma = 5$–18.3 MeV; measured 4π neutron yield, neutron multiplicities, and average energies for monoenergetic photons; $\sigma(E_\gamma,1n)$, $\sigma(E_\gamma,2n)$, $\sigma(E_\gamma,F)$, integrated cross sections and moments, GDR parameters, nuclear shape parameters, neutron and fission probabilities.]

I. INTRODUCTION

As Bohr pointed out (Ref. 1), photofission reactions make use of the simplicity and directness of the electromagnetic interaction as a powerful tool with which to explore the process of nuclear fission. However, owing to the difficulty of performing photofission measurements, especially with monoenergetic photons, very little accurate, detailed, and systematic data have been obtained. We have made a systematic study, part of which is reported here, in an effort to alleviate that situation.

The characteristics of the giant dipole resonance (GDR) for the actinide nuclei and the deformation parameters of these nuclei are of particular interest. For such high-Z, high-Coulomb-barrier nuclei, the total photon-absorption cross section $\sigma(\gamma,\text{tot})$, from which one can determine the (static) deformation parameters,[2,3] is, to a good approximation, equal to the sum of the photoneutron and photofission cross sections.

In a companion paper (Ref. 4), we have presented details of the experimental apparatus and techniques, descriptions of the enriched isotopic samples used, and the data-analysis procedures employed to extract the fission-multiplicity width parameter σ_p and the average number of prompt neutrons emitted in the photofission process $\bar{\nu}_p$ from the data. The resulting values for these parameters were presented in Ref. 4 in tabular and graphical form and were found to agree with those values for these quantities measured elsewhere. The analysis of the cross-section data here depends upon the ability to assign the detected reaction events to the various photoneutron and photofission channels based upon their measured neutron multiplicity and average neutron energy, which in turn depend upon the values employed for σ_p and $\bar{\nu}_p$. In this experiment these quantities were *measured*, not assumed as has been done in previous work of this kind.[5,6] Our values for the number of delayed neutrons per fission, measured by counting neutrons between beam bursts, also are presented in Ref. 4.

Work in the photofission field through the mid-70's is summarized in the review articles by Huizenga and Britt[7] and by Bhandari and Nascimento,[8] and is set in the framework of fission research in the book of Vandenbosch and Huizenga.[9] Since the first photofission measurements,[10,11] experimental cross-section work for the actinide nuclei studied here usually has fallen into one of two categories: (1) measurements at excitation energies in the GDR region and (2) measurements in the low-energy region near the fission barriers and (γ,n) thresholds. For the GDR energy region, there have been several bremsstrahlung measurements reported, primarily on ^{238}U and ^{232}Th with low resolution.[12–18] References 12–15 and 18 report photofission measurements and Refs. 13, 14, 16, and 17 report photoneutron

yield measurements. There have been only two GDR measurements performed with monoenergetic (positron-annihilation) photons; that of Bowman *et al.*[5] on ^{235}U and that of Veyssière *et al.*[6] on ^{238}U, ^{232}Th, and ^{237}Np. There has been one total photon-absorption measurement reported recently,[19] yielding $\sigma(\gamma, \text{tot})$ for ^{235,238}U, ^{232}Th, and ^{239}Pu.

Bremsstrahlung photofission cross-section measurements for the low-energy region have been reported by Katz *et al.*[18] and by Rabotnov and co-workers[20,21] on ^{238}U and ^{232}Th, among other nuclei; by Bowman *et al.*[22] on ^{238}U; by Zhuchko *et al.*[23] on ^{236}U; and by Lindgren *et al.*[24] on ^{234,236,238}U. Cross-section measurements performed with several monoenergetic or quasi-monoenergetic-photon sources have been reported also: by Huizenga *et al.*[25] on many actinide nuclei with $F(p, \alpha\gamma)$ photons; by Manfredini *et al.*[26] and by Mafra *et al.*[27] on ^{238}U and ^{232}Th and by Dragnev *et al.*[28] on ^{235,238}U, ^{232}Th, and ^{239}Pu with neutron-capture gamma rays; by Knowles and co-workers[29,30] on ^{235,238}U and ^{232}Th and by Morrison and co-workers[31,32] on ^{235,236,238}U and ^{232}Th with Compton-scattered neutron-capture gamma rays; and by Dickey and Axel[33] on ^{238}U and ^{232}Th with tagged bremsstrahlung photons. In addition to photofission data, Mafra *et al.*,[27] Knowles and Mafra,[30] and Dickey and Axel[33] also report photoneutron cross-section measurements.

II. EXPERIMENT AND DATA REDUCTION

The experimental method and data-reduction techniques employed in the present measurements are based upon those used in earlier photonuclear and photofission experiments by the Livermore[34,35] and Los Alamos[36] groups. A detailed description appears in Ref. 4. Briefly, the method consists of using a positron beam incident upon a low-Z target to produce photons by annihilation in flight. The narrowly collimated forward-going photons have an energy that depends only upon the energy of the incident positrons. The collimated photon beam passes through a xenon-filled spherical ion chamber, which serves as a flux monitor, and impinges on the photofission sample under study that is located at the center of a high-efficiency 4π neutron detector. The annihilation photons are accompanied by a continuous spectrum of photons from positron bremsstrahlung produced in the annihilation target. The contribution to the neutron yield owing to the latter, which is a smooth function of energy, is measured in a separate set of runs with incident electrons, and is subtracted out. Sample-blank backgrounds also are obtained from another set of runs and are taken into account in reducing the data. An on-line computer is used to collect, sort, and record the data.

The source of positrons for these measurements was a high-Z (W-Re) converter target, located at the end of the Livermore Electron-Positron Linear Accelerator, on which the high-current electron beam was focused. The positrons, produced by pair production in the converter, were passed through a bending-magnet-and-slit energy-defining system (the typical momentum spread accepted was 1%), transported to the experimental area, and focused onto the 0.076-cm-thick beryllium annihilation target. For the present measurements, the positron beam current was held to 0.1 nA in order to limit pile-up events. After traversing the annihilation target, the residual positron beam was swept through a 90° bend and dumped in a 5-m-deep hole. The forward-going photons were collimated to a circular beam with a half-angle of 7.24 mrad. In the present experiment the photon energy resolution ranged from about 250 keV at energies below 10 MeV to about 325 keV at the highest energy (~18 MeV).

The photofission samples were located at a distance of 310 cm from the annihilation target. Up to eight samples or blanks, including a standard Pu-Be neutron source used to monitor the detector efficiency, were loaded into the neutron detector sequentially with a remotely controlled sample changer, so that beam-tuning conditions remained

TABLE I. Photoneutron thresholds and photofission barriers.[a]

Nucleus	$E_{\text{thr}}(\gamma,n)$[b]	$E_{\text{thr}}(\gamma,2n)$[b]	$E_{\text{thr}}(\gamma,3n)$[b]	$B_F(\gamma,f)$[c]	$B_F(\gamma,nf)$[d]
^{235}U	5.298	12.141	17.894	5.8	11.3
^{236}U	6.546	11.844	18.688	5.9	12.3
^{238}U	6.153	11.278	17.824	5.8	12.3
^{232}Th	6.436	11.557	18.348	6.0	12.6

[a] All quantities in MeV.
[b] From Ref. 37.
[c] First-chance fission barrier, from Ref. 9, p. 255; all values ±0.2 MeV.
[d] Second-chance fission barrier, from adding the value for $E_{\text{thr}}(\gamma,n)$ to that for $B_F(\gamma,f)$ for the $(N-1)$ nucleus from Ref. 9, p. 255; all values ±0.2 MeV.

the same for different samples at a given energy. The actinide sample specifications are given in Ref. 4; the photonuclear thresholds[37] for these nuclei are listed in Table I. All photonuclear thresholds determined in the present experiment (see Sec. III B) agree, within the experimental limits, with those given in Table I. As a check on all aspects of the experimental calibration and monitoring, a sample of ^{141}Pr was used along with the actinide samples, and the absolute cross section obtained was compared with the results of previous measurements.[38-41] The ^{141}Pr total photoneutron cross section (11–14 MeV) determined here agreed to within ±5% with all of the previous results.[2]

The neutron detector consists of a 61-cm cube of paraffin moderator in which are embedded 48 51-cm-long BF_3 proportional counters. The latter are arranged in an array of four coaxial rings, each containing 12 counters, cylindrically symmetric about the beam line. For each annihilation-photon energy the number of neutron counts in each ring is measured, which provides not only the raw counting rates necessary for computing the cross sections, but also the average neutron energy that is determined by the ratio of counts in the outer and inner rings of BF_3 tubes (the "ring ratio"). The on-line computer recorded the number of events in which one, two, three, etc., neutrons were detected within the gate and the ring distribution for each category of event. Thus ring ratios, and therefore the detector efficiency, could be determined separately for multiple-neutron as well as for single-neutron events. For these photofission experiments, this neutron-multiplicity counting technique was modified to account simultaneously and independently for (γ, n), $(\gamma, 2n)$, and (γ, F) events. The method by which $\bar{\nu}_p(E_\gamma)$ was determined is discussed in detail in Refs. 4 and 36. Briefly, $\bar{\nu}_p(E_\gamma)$ is determined from the observed neutron multiplicity at each E_γ. The fission neutron-multiplicity model of Terrell[42] is used in the analysis of these data.

The data-analysis procedures and discussions of the experimental uncertainties are given in detail elsewhere.[2,4,35,36,43] Statistical uncertainties are reflected in the error bars on the data points. Systematic uncertainties arising from the subtraction of the positron-bremsstrahlung yields, from the neutron-detector efficiency calibration, and from the photon-flux calibration are about 2%, 3%, and 5%, respectively. Impurities in the samples[4] have been accounted for whenever their effect on the results exceeded 1%. Multiplication effects in the samples were determined both by Monte Carlo calculations and by measurements with samples wrapped in thin cadmium metal foil; such effects necessitated small corrections to the data of 5%, 2%, 1%, and 0.5% for ^{235}U, ^{236}U, ^{239}U, and ^{232}Th, respectively. Uncertainties resulting from these corrections are estimated to be less than 1% in all cases. The final cross-section values are subject to overall systematic uncertainties that do not exceed 7%. The statistical uncertainties for the total photonuclear cross sections were computed by adding in quadrature those for the partial cross sections.

III. RESULTS AND DISCUSSION

A. Average photofission neutron energies

The average neutron energies $\bar{E}_n$ for those neutrons emitted in the photofission process below $B_F(\gamma, nf)$ are shown in Fig. 1, plotted as a function of $\bar{\nu}_p$. These values have been obtained from the coincidence ring-ratio data discussed in detail in Ref. 4. Values for each of the isotopes are shown with separate symbols. A range in photofission $\bar{\nu}_p$ from 1.8 to 3.3 is covered. The solid curve shown is the evaporation-model prediction of Terrell.[42] As discussed in Ref. 4, only the ring-ratio data below $B_F(\gamma, nf)$ can be compared appropriately with Terrell's prediction. Above $B_F(\gamma, nf)$ the coincidence ring ratio includes contributions from second-chance fission reactions. The coincidence ring ratio for photofission reactions above $B_F(\gamma, nf)$ is discussed in detail in Ref. 4. The coincidence ring-ratio data for the (γ, n) and $(\gamma, 2n)$ reactions are discussed in Refs. 4 and 44.

B. Cross sections

The photonuclear cross sections for ^{235}U, ^{236}U, ^{238}U, and ^{232}Th are shown, as functions of photon

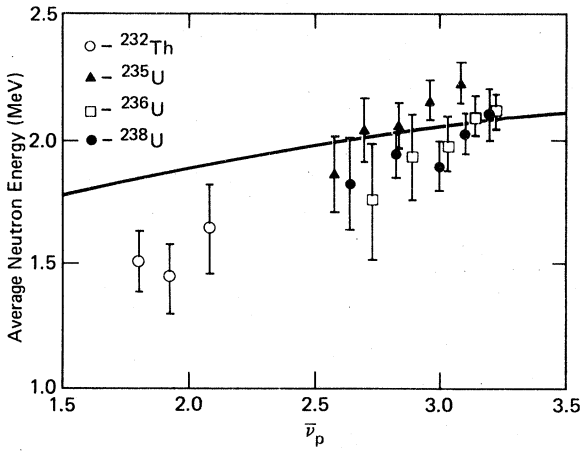

FIG. 1. Average neutron energy from the coincidence ring-ratio data for (γ, f) reactions, plotted as a function of $\bar{\nu}_p$. The smooth curve is the evaporation theory prediction of Terrell (Ref. 42).

energy, in Figs. 2–5, respectively. The total photonuclear cross sections $\sigma(\gamma, \text{tot}) = \sigma[(\gamma, n) + (\gamma, 2n) + (\gamma, F)]$ [Figs. 2(a), 3(a), 4(a), and 5(a)] all have about the same peak cross-section value, except for ^{236}U, which is approximately 10% smaller. These cross sections also have roughly the same shape, although there is not as pronounced a minimum atop the GDR for ^{232}Th as there is for the rest. The maximum cross sections all are about 0.5 b and all are about 6 MeV wide; they clearly are split in the fashion of other

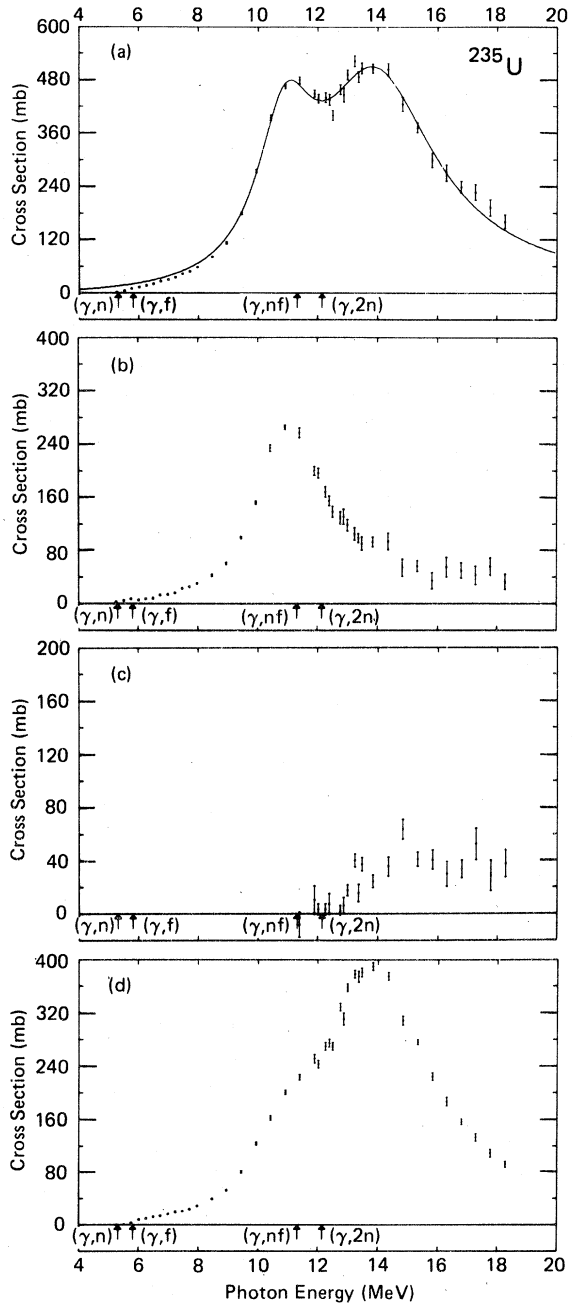

FIG. 2. Photonuclear cross sections for ^{235}U: (a) total photonuclear cross section $\sigma(\gamma, \text{tot}) = \sigma[(\gamma, n) + (\gamma, 2n) + (\gamma, F)]$, together with a two-component Lorentz-curve fit to the data in the GDR energy region; (b) single-photoneutron cross section $\sigma(\gamma, n)$; (c) double-photoneutron cross section $\sigma(\gamma, 2n)$; (d) photofission cross section $\sigma(\gamma, F)$.

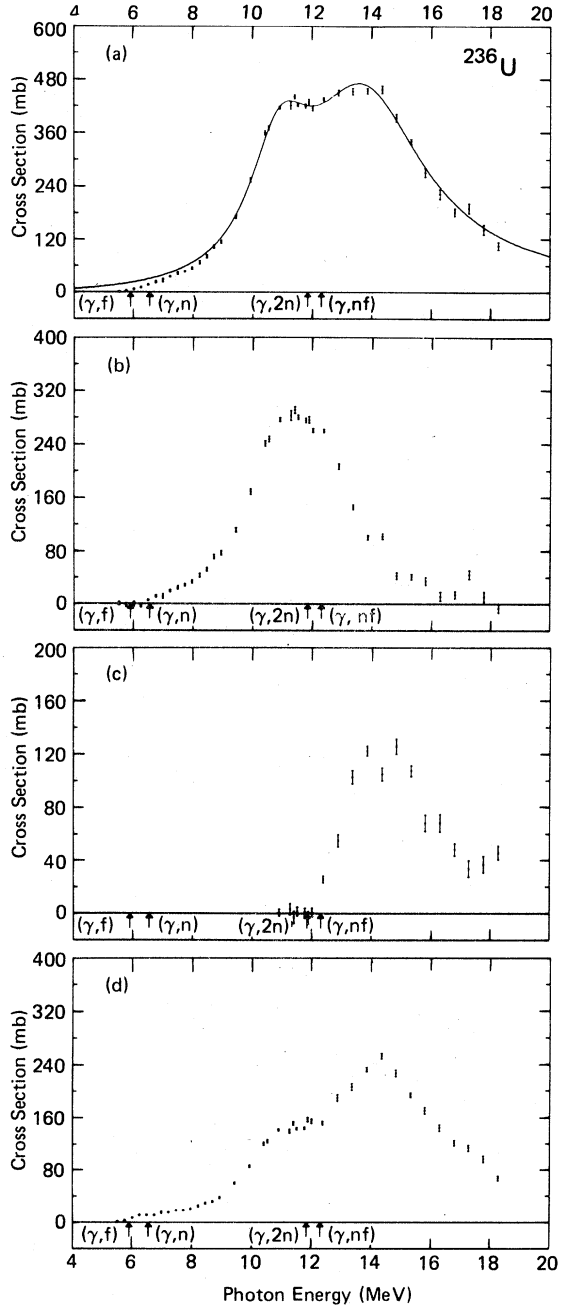

FIG. 3. Photonuclear cross sections for ^{236}U: (a) $\sigma(\gamma, \text{tot})$, with a Lorentz-curve fit; (b) $\sigma(\gamma, n)$; (c) $\sigma(\gamma, 2n)$; (d) $\sigma(\gamma, F)$.

statically deformed nuclei.[2,45,46] All have been fitted with two-component Lorentz curves (more on this in Sec. III C). No obvious structure, other than the GDR itself, appears in these cross sections, except near the (γ, n) thresholds (see Sec. III E).

The single-photoneutron cross sections $\sigma(\gamma, n)$ are shown in Figs. 2(b), 3(b), 4(b), and 5(b). Note that the measured $\sigma(\gamma, n)$ includes $\sigma(\gamma, pn)$ and $\sigma(\gamma, \alpha n)$, but these cross sections are expected to be very small below 18 MeV because of the Coulomb barrier, not to mention the competition from the photofission channels. The size of the cross section varies widely for these nuclei, and $\sigma(\gamma, n)$ for ^{235}U and ^{236}U, being smaller, are plotted on a

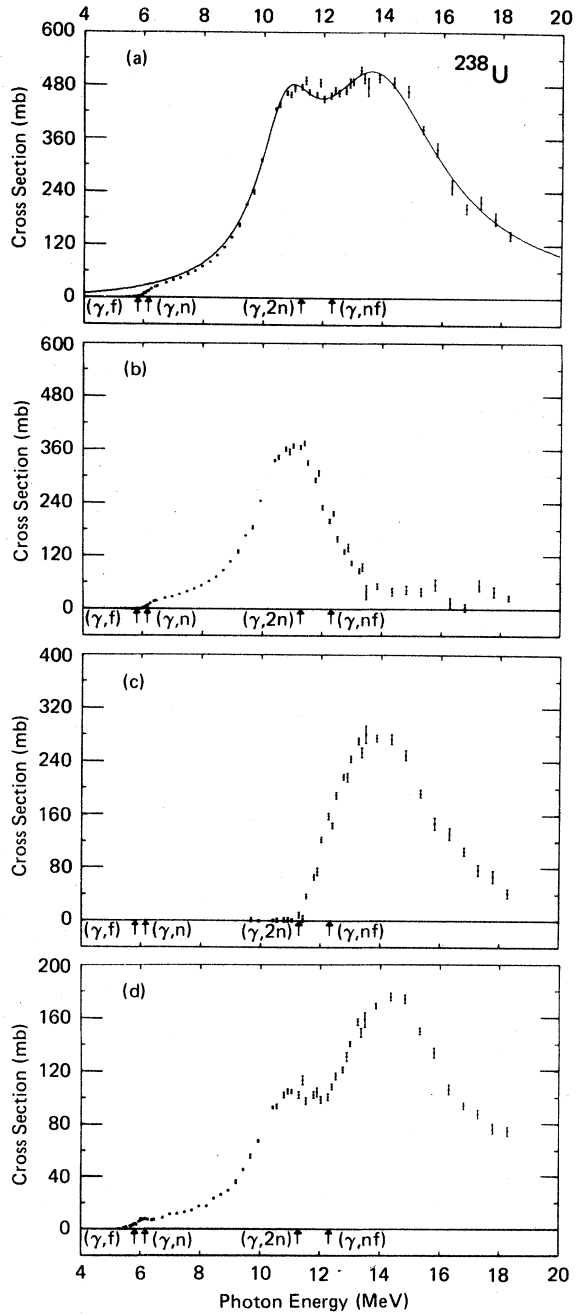

FIG. 4. Photonuclear cross sections for ^{238}U: (a) $\sigma(\gamma, \text{tot})$, with a Lorentz-curve fit; (b) $\sigma(\gamma, n)$; (c) $\sigma(\gamma, 2n)$; (d) $\sigma(\gamma, F)$.

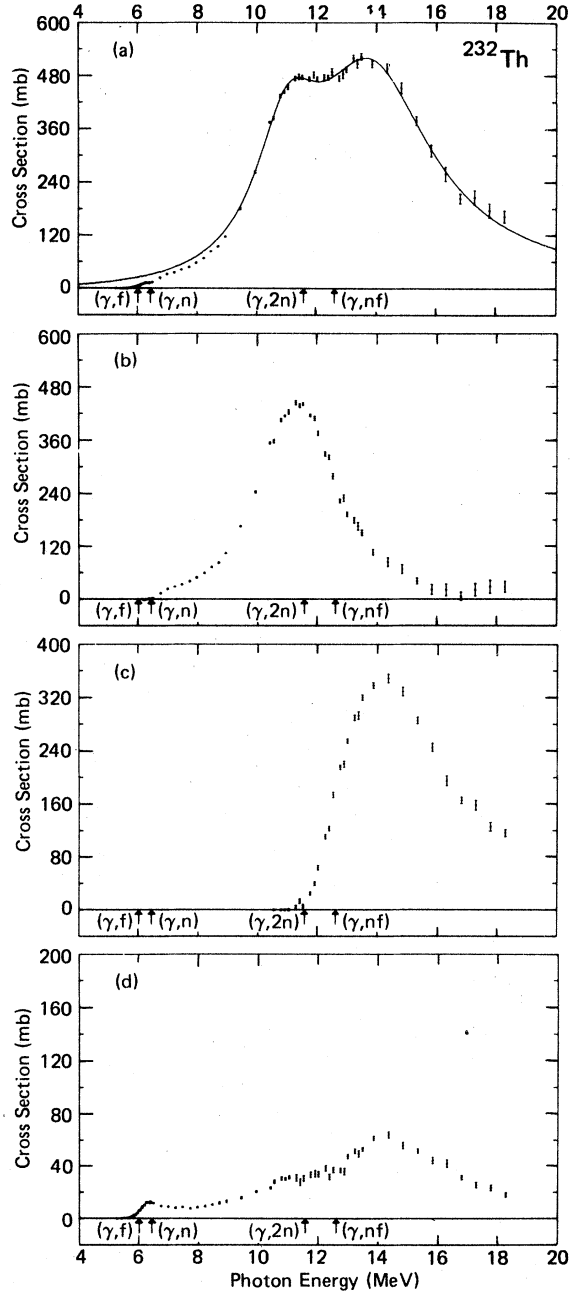

FIG. 5. Photonuclear cross sections for ^{232}Th: (a) $\sigma(\gamma, \text{tot})$, with a Lorentz-curve fit; (b) $\sigma(\gamma, n)$; (c) $\sigma(\gamma, 2n)$; (d) $\sigma(\gamma, F)$.

more expanded scale than is used for ^{238}U and ^{232}Th. If the total photon-absorption cross sections are roughly the same—sum-rule considerations dictate that they should be—and if the photofission cross sections vary as the nuclear fissionability Z^2/A (see Sec. III F), then we expect the photoneutron cross sections to be smallest for ^{235}U and largest for ^{232}Th; we see from Figs. 2–5 that this is so. The (γ, n) cross sections fall sharply above the $(\gamma, 2n)$ and (γ, nf) thresholds, as is the case for essentially all other medium and heavy nuclei.[2,46] None of the (γ, n) cross sections has the double-humped shape characteristic of deformed nuclei, and thus a measurement of $\sigma(\gamma, n)$ alone (by activation, for example) would not yield even a rough idea of the deformation parameters for these nuclei.

The $(\gamma, 2n)$ cross sections, shown in Figs. 2(c), 3(c), 4(c), and 5(c), also grow with decreasing fissionability and are plotted accordingly with appropriate scales. This behavior is quite dramatic: $\sigma(\gamma, 2n)$ for ^{232}Th is about four times the size of $\sigma(\gamma, 2n)$ for ^{235}U (see Sec. III D for details of the integrated cross sections).

The photofission cross sections $\sigma(\gamma, F) = \sigma[(\gamma, f) + (\gamma, nf)]$, shown in Figs. 2(d), 3(d), 4(d), and 5(d), again are plotted using scales that differ by a factor of 2. The increase of $\sigma(\gamma, F)$ with fissionability is even more striking: $\sigma(\gamma, F)$ for ^{235}U is fully five times the size of $\sigma(\gamma, F)$ for ^{232}Th (Sec. III D). Again we notice that a measurement of only one photonuclear channel would give a distorted and erroneous view of the shape of the GDR; we see that $\sigma(\gamma, F)$ alone would lead to values for the ratio of the areas R_A of the first to the second hump of the GDR that are much too small (see Sec. III C). Another feature of the (γ, F) cross sections is that for all four nuclei, $\sigma(\gamma, F)$ rises sharply just above the second-chance fission barrier $B_F(\gamma, nf)$; it is not surprising that $\sigma(\gamma, F)$ is enhanced when this new channel opens. Finally, although the (γ, F) cross sections are relatively structureless except for the GDR, we see relatively large peaks in $\sigma(\gamma, F)$ for ^{238}U and ^{232}Th just below the (γ, n) thresholds, apparently arising from competition between the fission and neutron channels (see Secs. III E and III F).

TABLE III. Parameters for classical theories.[a]

Nucleus	E_m[b]	α[c]	β[d]	K[e]
^{235}U	12.94	79.8	32.1	27.3±0.7
^{236}U	12.82	79.2	31.9	27.0±0.5
^{238}U	12.79	79.3	31.8	27.1±0.6
^{232}Th	12.93	79.4	32.0	26.9±0.5

[a] All quantities given in MeV.
[b] Mean energy of the GDR, defined by Eq. (5).
[c] Hydrodynamic parameter, defined by $E_m = \alpha A^{-1/3}$.
[d] Collective parameter, defined by $E_m = \beta A^{-1/6}$.
[e] Nuclear symmetry energy, computed from Eq. (2).

C. Giant-resonance parameters

The classic collective description of the GDR predicts that the total photon-absorption cross section $\sigma(\gamma, \text{tot})$ for statically deformed nuclei is characterized as the sum of two Lorentz-shaped curves,

$$\sigma(\gamma, \text{tot}) = \sum_{i=1}^{2} \left\{ \sigma_m(i) \Big/ \left(1 + \frac{[E_\gamma^2 - E_m^2(i)]^2}{E_\gamma^2 \Gamma^2(i)} \right) \right\}, \quad (1)$$

where $\sigma_m(i)$, $E_m(i)$, and $\Gamma(i)$ are the peak height, resonance energy, and full width of the ith Lorentz curve. Accordingly, the (γ, tot) cross sections in Figs. 2(a), 3(a), 4(a), and 5(a) have been fitted with two-component Lorentz curves. The fitting interval used for all four nuclei was 9 to 18 MeV, which includes easily the entire GDR region. The resulting fits to the data are shown in the figures and the Lorentz parameters of these fitted curves are given, together with their statistical uncertainties, in Table II.

Values of the parameters for the classical theories are given in Table III. These include α and β, the proportionality constants characterizing the mean GDR energy E_m with mass number, and K, the nuclear symmetry energy computed from the relation[3]

TABLE II. Parameters of Lorentz-curve fits to the giant dipole resonance.[a]

Nucleus	$E_m(1)$ (MeV)	$\sigma_m(1)$ (mb)[b]	$\Gamma(1)$ (MeV)	$E_m(2)$ (MeV)	$\sigma_m(2)$ (mb)[b]	$\Gamma(2)$ (MeV)
^{235}U	10.90±0.05	328±19	2.30±0.15	13.96±0.09	459±10	4.75±0.32
^{236}U	10.92±0.04	271±16	2.55±0.17	13.78±0.08	415±10	4.88±0.24
^{238}U	10.77±0.04	311±20	2.37±0.13	13.80±0.09	459± 9	5.13±0.35
^{232}Th	11.03±0.04	302±19	2.71±0.13	13.87±0.08	449± 9	4.77±0.28

[a] Lorentz parameters defined by Eq. (1); the fitting interval for all cases is 9 to 18 MeV.
[b] Uncertainties for σ_m given here are relative. The absolute uncertainties are 7%.

$$K = 9.935 \times 10^{-4} \frac{A^{8/3}}{NZ} \frac{[E_m(1)]^2}{1-[\Gamma(1)/2E_m(1)]^2} \times \frac{\eta^{4/3}}{(1+0.018\,60\epsilon - 0.033\,14\epsilon^2)^2}, \quad (2)$$

where η is the nuclear deformation parameter, defined as the ratio of the semimajor axis b to the semiminor axis a of the (prolate) deformed nucleus, and computed from the relation[3]

$$E_m(2)/E_m(1) = 0.911\eta + 0.089, \quad (3)$$

and ϵ is the nuclear eccentricity, defined as $(b^2 - a^2)/R^2$, where R is the radius of a sphere of equal volume (for a prolate spheroid, $R^3 = a^2 b$), and computed from the resulting relation

$$\epsilon = (\eta^2 - 1)\eta^{-2/3}. \quad (4)$$

The value for E_m for a prolate spheroid should be given by

$$E_m = [E_m(1) + 2E_m(2)]/3, \quad (5)$$

two-thirds of the way from the lower- to the higher-energy peak of the GDR; this value has been adopted for all the nuclei studied here. The present values both for K and for E_m follow very well indeed the systematics for these quantities discussed at length in Ref. 2.

Values for various nuclear shape parameters, computed from the Lorentz parameters of Table II, are given in Table IV. These are R_A, the area ratio defined as

$$R_A = \sigma_m(1)\,\Gamma(1)/\sigma_m(2)\,\Gamma(2) \quad (6)$$

and predicted to be one-half for prolate nuclei; η, the deformation parameter of Eq. (3); ϵ, the nuclear eccentricity of Eq. (4); β_2, a deformation parameter more commonly used than η or ϵ, defined as

$$\beta_2 = \tfrac{2}{3}(\pi/5)^{1/2}\epsilon \cong 0.53\epsilon, \quad (7)$$

and Q_0, the intrinsic quadrupole moment defined as

$$Q_0 = \tfrac{2}{5} ZR^2\epsilon, \quad (8)$$

where the equivalent nuclear radius $R = R_0 A^{1/3}$. The photonuclear approach yields the eccentricity ϵ of the nuclear matter distribution while the Coulomb-excitation approach yields a parameter that describes the shape of the charge distribution. Also, R_A is not equal to the hydrodynamic prediction of one-half; rather, a value close to one-third is indicated in Table IV. We have no ready explanation for this feature of the data; similar behavior occurs for nuclei on the fringes, rather than in the center, of the deformed rare-earth region.[45]

Values for Q_0 computed from Eq. (8) with R_0 taken to be 1.20 fm are given in the sixth column of Table IV, while values for Q_0 determined by other experimental methods[47] are given in the seventh column. The latter are substantially smaller than the former, even allowing for experimental uncertainties; we therefore normalize the average of the former to that of the latter (column 8 of Table IV). This procedure results in an average value for R_0 of 1.15 fm for these actinide nuclei, in contrast to the deformed rare-earth nuclei studied earlier,[45] where the same procedure resulted in an average value for R_0 of 1.26 fm. The present experiment measures ϵ; if we accept the values of Q_0 from Ref. 47, and assume a purely rotational model for these nuclei (i.e., the hexadecapole deformation β_4 is neglected), then we have determined that R_0 for these actinide nuclei is appreciably smaller than for the rare-earth nuclei reported on in Ref. 45.

D. Integrated cross sections

The integrated cross sections measured in this experiment are summarized in Table V. Columns 2, 3, and 4 in this table list the integrated (up to $E_{\gamma\,\max} = 18.3$ MeV) single- and double-photoneutron and photofission cross sections, respectively; column 5 lists the total area under the two-com-

TABLE IV. Nuclear shape parameters.

Nucleus	R_A[a]	η[b]	ϵ[c]	β_2[d]	Q_0 (b)[e]	Q_0 (b)[f]	Q_0 (b)[g]
^{235}U	0.35	1.308	0.595	0.315	12.0	10.6 ±0.2	11.0±0.5
^{236}U	0.34	1.287	0.556	0.295	11.2	10.75±0.7	10.3±0.4
^{238}U	0.31	1.309	0.596	0.316	12.1	11.3 ±0.1	11.1±0.5
^{232}Th	0.38	1.283	0.547	0.290	10.7	9.8 ±0.1	9.8±0.4

[a] Area ratio, defined by Eq. (6).
[b] Deformation parameter, computed from Eq. (3).
[c] Nuclear eccentricity, computed from Eq. (4).
[d] Deformation parameter, computed from Eq. (7).
[e] Intrinsic quadrupole moment, computed from Eq. (8), with R_0 taken to be 1.20 fm.
[f] Intrinsic quadrupole moment, taken from Ref. 47.
[g] "Best value" for Q_0, computed from Eq. (8), with R_0 taken to be 1.15 fm (see text).

TABLE V. Integrated cross sections.[a]

Nucleus	$\sigma_{\rm int}(\gamma,n)$ (MeV b)	$\sigma_{\rm int}(\gamma,2n)$ (MeV b)	$\sigma_{\rm int}(\gamma,F)$ (MeV b)	$\frac{\frac{1}{2}\pi[\sigma_m(1)\Gamma(1)+\sigma_m(2)\Gamma(2)]}{0.06NZ/A}$[b]
^{235}U	1.14	0.20	2.16	1.37
^{236}U	1.26	0.45	1.45	1.26
^{238}U	1.36	1.13	1.09	1.43
^{232}Th	1.66	1.45	0.37	1.41

[a] $\sigma_{\rm int}(\gamma,x)=\int\sigma(\gamma,x)dE_\gamma$, integrated from threshold to the maximum experimental energy $E_{\gamma\max}=18.3$ MeV.
[b] Uncertainties given here are relative. The absolute uncertainties are 7%.

ponent Lorentz-curve fits to $\sigma(\gamma,\text{tot})$ in TRK sum-rule units. The values listed in column 5 give an indication of the maximum amount of exchange-force enhancement of the dipole sum-rule values that might be needed to account for the GDR. The result for ^{236}U agrees with the systematic result of 1.21 ± 0.11 sum-rule units of Ref. 2 whereas the results for the other nuclei studied here lie rather higher, but still within the range of many other nuclei studied.[2]

The integrated moments of the measured total photonuclear cross sections σ_{-1} and σ_{-2} are given in columns 2 and 4, respectively, of Table VI. Migdal[48] derived a sum rule for σ_{-2} based upon the assumption of a constant nuclear (but variable neutron and proton) density. The value of σ_{-2}, which is proportional to the nuclear polarizability, is predicted to be[49]

$$\sigma_{-2}=0.05175A^{5/3}/K \text{ mb MeV}^{-1} \quad (9)$$

for spherical nuclei, where K is in MeV and $R_0=1.20$ fm; for $K=23$ MeV, $\sigma_{-2}=0.00225A^{5/3}$ mb MeV^{-1}. Column 5 of Table VI shows that the experimental values lie within 20% of this prediction. If instead of the constant 23 MeV, however, the values for K given in Table III are used, column 6 of Table VI shows that the agreement for this case is not nearly as good. Indeed, the values of the nuclear symmetry energy computed from the values for σ_{-2} by use of Eq. (9), listed in the last column of Table VI, differ from those in Table III by an average of 30%. Because such a discrepancy is not observed for nuclei that have no equilibrium deformation,[2,34,50] where the two methods for computing K yield essentially the same results, the discrepancy observed here can be taken as another indication that these actinide nuclei are strongly statically deformed.

The present experimental data on all the integrated cross sections and their moments are shown in Figs. 6–9 in the form of running sums of the quantities plotted as functions of the photon energy up to which they are integrated. This form of displaying the integrated cross-section data is useful for information-retrieval purposes, and also shows whether the various plotted quantities approach asymptotic behavior at the highest photon energies measured. These figures show that the integrated cross sections and their moments do not approach asymptotic values, except for the (γ,n) channel, but this probably reflects the fact that the present measurements were carried out only up to $E_{\gamma\,\max}=18.3$ MeV. A more important feature to be noted in Figs. 6–9 is the occurrence of the various crossovers of the curves, unique to fissionable nuclei, as discussed in Sec. III B.

E. Comparison with other experiments

1. *The GDR energy region*

Measurements of photofission and photoneutron yield cross sections made prior to the 1960's

TABLE VI. Integrated cross-section moments.[a]

Nucleus	σ_{-1} (mb)	$\sigma_{-1}A^{-4/3}$ (mb)	σ_{-2} (mb MeV^{-1})	$\frac{\sigma_{-2}}{0.00225A^{5/3}}$	$\frac{\sigma_{-2}K}{0.05175^{5/3}}$	$\frac{0.05175A^{5/3}}{\sigma_{-2}}$ (MeV)
^{235}U	278	0.191	23.1	1.15	1.36	20.1
^{236}U	252	0.173	21.0	1.04	1.21	22.2
^{238}U	286	0.194	24.0	1.17	1.38	19.7
^{232}Th	276	0.194	22.8	1.16	1.35	19.9

[a] $\sigma_{-1}=\int\sigma(\gamma,\text{tot})\,E_\gamma^{-1}\,dE_\gamma$ and $\sigma_{-2}=\int\sigma(\gamma,\text{tot})E_\gamma^{-2}\,dE_\gamma$, integrated from threshold to $E_{\gamma\max}=18.3$ MeV.

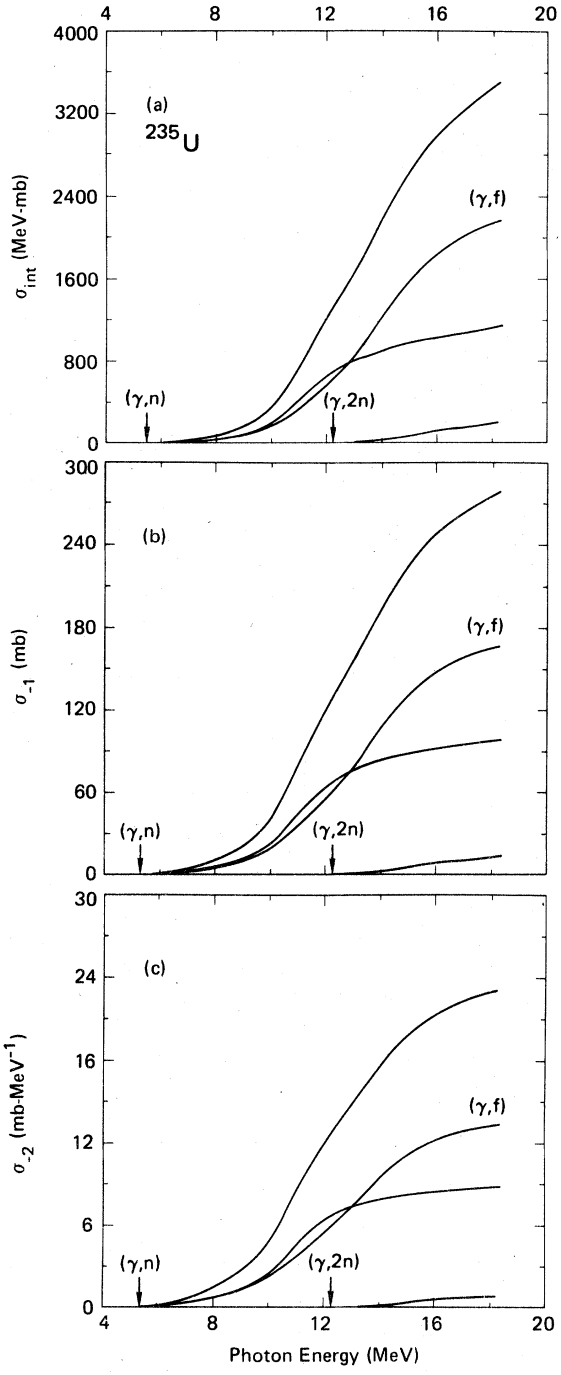

FIG. 6. Running sums of integrated cross sections and their moments plotted versus the upper-energy limit of integration, for ^{235}U: (a) integrated cross sections σ_{int} for (γ,tot), (γ,n), $(\gamma,2n)$, and (γ,F) reactions; (b) first moment of the integrated cross sections σ_{-1}; (c) second moment of the integrated cross sections σ_{-2}.

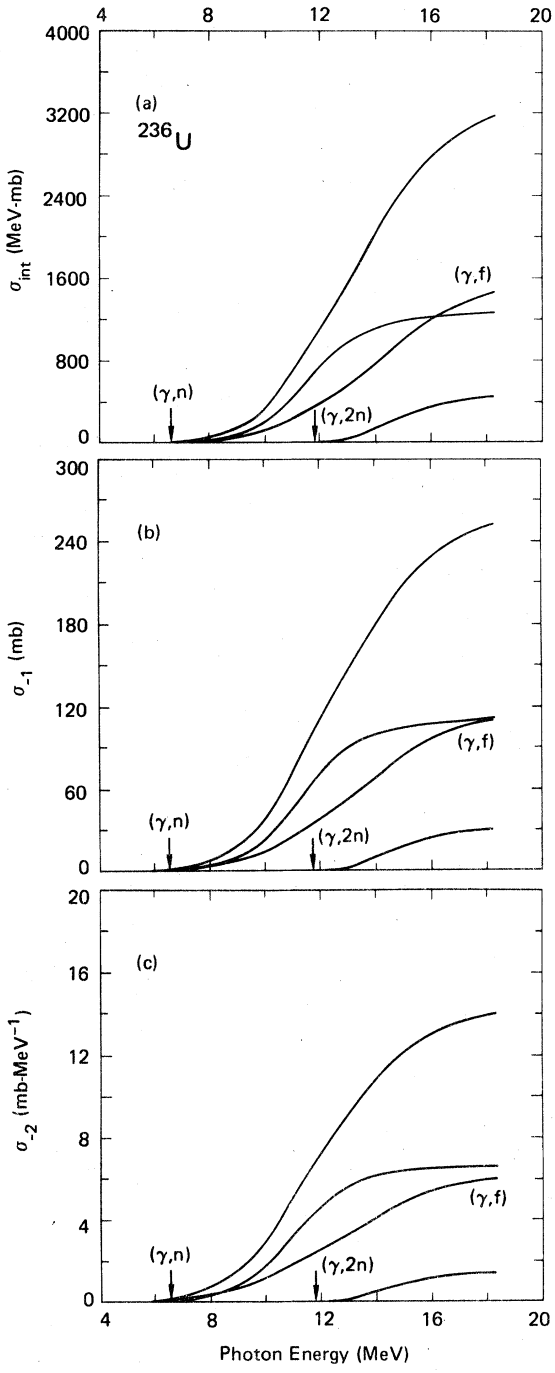

FIG. 7. Running sums of integrated cross sections and moments for ^{236}U: (a) σ_{int}; (b) σ_{-1}; (c) σ_{-2}.

(Refs. 12–18) are neither accurate nor detailed enough to be compared profitably with the present data. The annihilation-photon experiment of Bowman *et al.*[5] was performed with a fission ionization chamber to detect fission fragments and with a 4π neutron detector having an efficiency of only 18% to detect neutrons. The values for $\sigma(\gamma,F)$ reported in Ref. 5 are scarcely one-half those presented here. The origin of this dis-

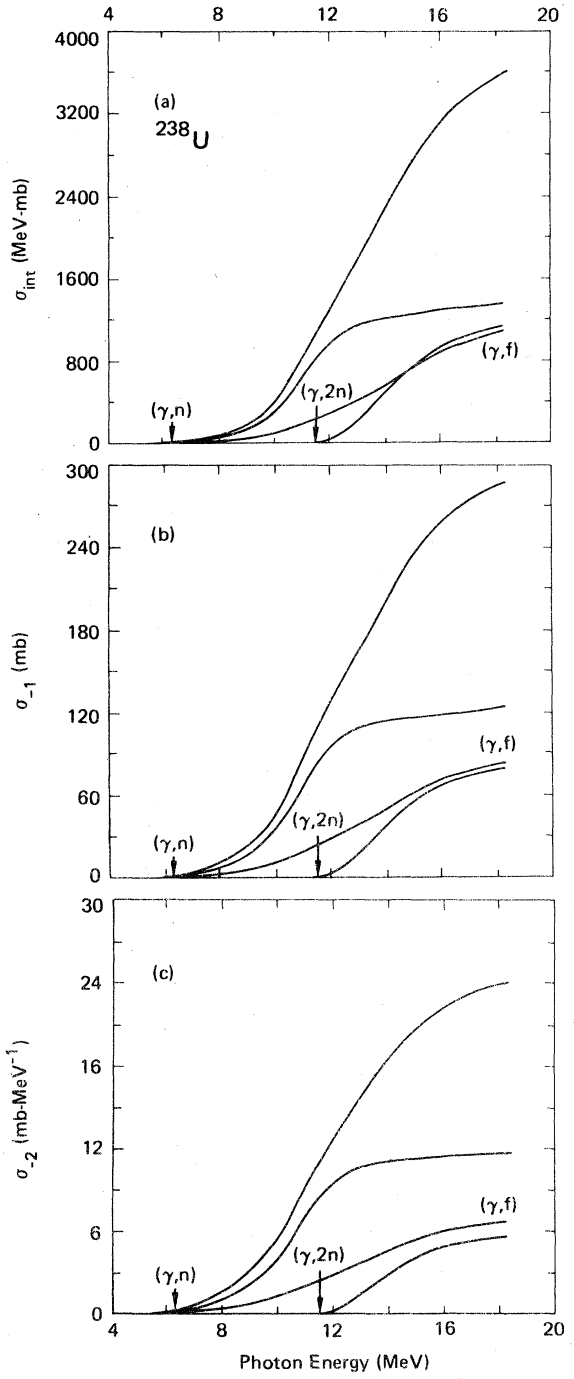

FIG. 8. Running sums of integrated cross sections and moments for ^{238}U: (a) σ_{int}; (b) σ_{-1}; (c) σ_{-2}.

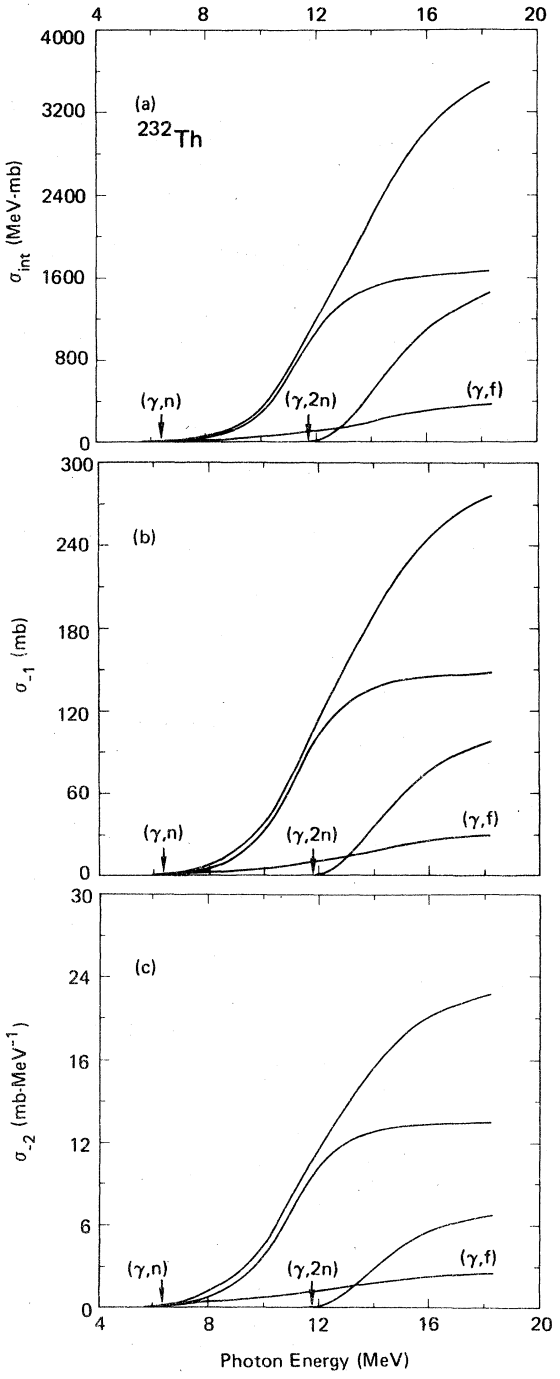

FIG. 9. Running sums of integrated cross sections and moments for ^{232}Th: (a) σ_{int}; (b) σ_{-1}; (c) σ_{-2}.

crepancy is not known, because the measured neutron yield cross section is in reasonable agreement with the present data; this indicates that the neutron-detector efficiency and photon-flux calibration of Ref. 5 probably are not responsible for the discrepancy. Also, the values assumed for $\bar{\nu}_p(E_\gamma)$ in Ref. 5 agree with our measured values (Ref. 4) in the GDR region. The lower values for $\sigma(\gamma, F)$ of Ref. 5 consequently result in values for $\sigma(\gamma, n)$ and $\sigma(\gamma, 2n)$ that are far in excess of the present values.

The annihilation-photon experiment of Veyssière

et al.[6] was performed in much the same way as the present work, except that the authors of Ref. 6 assumed values for $\bar{\nu}_p(E_\gamma)$ instead of measuring them. For ^{238}U and ^{232}Th, the values assumed by Veyssière *et al.*[6] lie substantially higher than our measured ones.[4] This results in lower values for the cross sections in the GDR region; in terms of integrated total cross sections, the values of Ref. 6 for both ^{238}U and ^{232}Th are about 10% lower than the present results. Still, the overall shapes of the cross sections of Ref. 6 are similar to the present results, especially for ^{238}U. Another way to compare the present data with those of Ref. 6 is to list the Lorentz parameters of the latter when they are fitted in the same way as the former (Table II). These parameters are listed in Table VII. Of course, if the data of Ref. 6 were reanalyzed using our measured values for $\bar{\nu}_p(E_\gamma)$, these parameters might change somewhat.

The photon-absorption measurements of $\sigma(\gamma, \text{tot})$ of Gurevich *et al.*[19] yield results for ^{235}U, ^{238}U, and ^{232}Th that, like the results of Ref. 6, all are about 10% smaller than the present results. The uncertainties quoted in Ref. 19 are 10 to 13%, which, added to the 7% uncertainties for the present measurement, place the two sets of data in agreement within the experimental limits. The overall shapes of the cross sections of Ref. 19 are likewise similar to the present results, especially for ^{238}U; the Lorentz parameters for the data of Ref. 19 also are given for comparison purposes in Table VII. However, the subtraction of the large atomic absorption (50 to 100 times the photonuclear absorption) for these high-Z atoms makes the total photon-absorption measurements difficult.

Comparing the values of the Lorentz parameters in Tables II and VII, we see better agreement among the various measurements than could have been expected in the light of the difficulties discussed above. However, the statistical uncertainties attached to the values of these parameters from Ref. 19 and to those for ^{232}Th from Ref. 6 are considerably larger than those for the present measurement.

2. *The low-energy region*

The photofission cross sections for the energy region below 9 MeV are plotted in Fig. 10 with an expanded cross-section scale so that the details of the data can be seen clearly. Although comparison of the present results with cross-section data obtained by unfolding bremsstrahlung spectra yields satisfactory agreement, most bremsstrahlung experiments were not undertaken to obtain absolute cross sections, but rather to measure the angular distributions of the fission fragments or the cross-section shapes at very low energies. In particular, the recent results of Zhuchko *et al.*[23] and of Lindgren *et al.*[24] on ^{236}U and ^{238}U are in agreement with the present data.

The results of high-resolution monoenergetic-photon measurements performed with nuclear gamma rays agree with the present data for some cases, but do not for others. The cross sections reported by Huizenga *et al.*[25] for the uranium isotopes are higher than ours, but for ^{232}Th agree very well. Those reported by Manfredini *et al.*,[26] Mafra *et al.*,[27] and Dragnev *et al.*[28] are in general agreement for ^{238}U, and for Ref. 28 for ^{235}U as well, but fall much lower than the present results for ^{232}Th. However, these measurements are of such high resolution (comparable to or smaller than the spacing between levels in the compound nucleus) that the data points measured could easily coincide with peaks or valleys in the underlying fine structure of the cross sections, so that direct comparison with the present data is not possible.

The quasi-monoenergetic-photon measurements performed with Compton-scattered gamma rays yield results that are all in poor agreement with the present data. These results, from Chalk River[29] and Iowa State,[31,32] shown as dashed and dot-dashed lines in Fig. 10, are generally much

TABLE VII. Lorentz parameters for other experiments.[a]

Nucleus	$E_m(1)$ (MeV)	$\sigma_m(1)$ (mb)[b]	$\Gamma(1)$ (MeV)	$E_m(2)$ (MeV)	$\sigma_m(2)$ (mb)[b]	$\Gamma(2)$ (MeV)	Ref. No.
^{235}U	10.74±0.20	284±43	3.43±0.70	13.77±0.26	342±41	4.82±0.64	19
^{238}U	10.94±0.03	296± 7	2.65±0.10	14.00±0.04	381± 5	4.59±0.11	6
^{238}U	10.95±0.13	273±32	2.84±0.47	14.19±0.21	363±23	5.27±0.55	19
^{232}Th	11.26±0.21	283±34	4.32±0.62	14.18±0.17	306±39	4.48±0.55	6
^{232}Th	10.88±0.23	252±34	3.90±0.71	13.87±0.18	352±38	4.47±0.46	19

[a] The fitting interval for all cases is 9 to 18 MeV.

[b] Uncertainties for σ_m given here are relative. The absolute uncertainties would include systematic as well as statistical uncertainties.

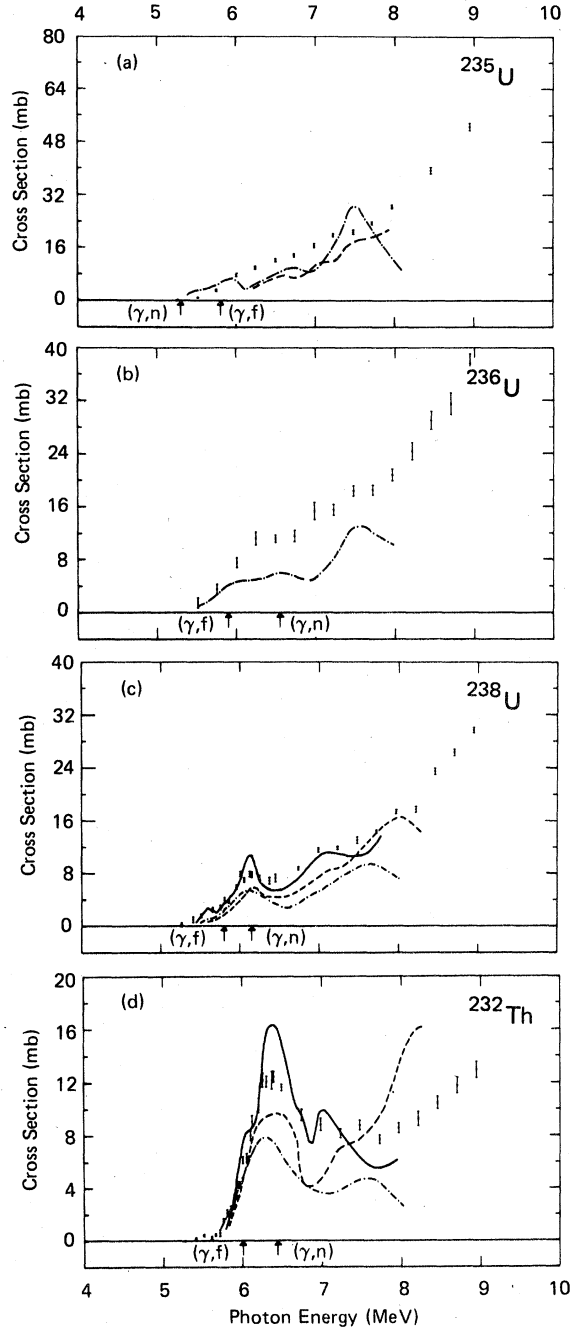

FIG. 10. Low-energy photofission cross sections: (a) $\sigma(\gamma,f)$ for ^{235}U: data points—present work, dashed curve—Chalk River (Ref. 29), dot-dashed curve—Iowa State (Ref. 32); (b) $\sigma(\gamma,f)$ for ^{236}U: data points—present work, dot-dashed curve—Iowa State (Ref. 31); (c) $\sigma(\gamma,f)$ for ^{238}U: data points—present work, dashed curve—Chalk River (Ref. 29), dot-dashed curve—Iowa State (Ref. 32), solid curve—Illinois (Ref. 33); (d) $\sigma(\gamma,f)$ for ^{232}Th: data points—present work, dashed curve—Chalk River (Ref. 29), dot-dashed curve—Iowa State (Ref. 31), solid curve—Illinois (Ref. 33).

lower than our results and frequently contain structure not seen in the present data, especially in the case of ^{235}U as shown in Fig. 10(a).

The monoenergetic-photon measurements per-

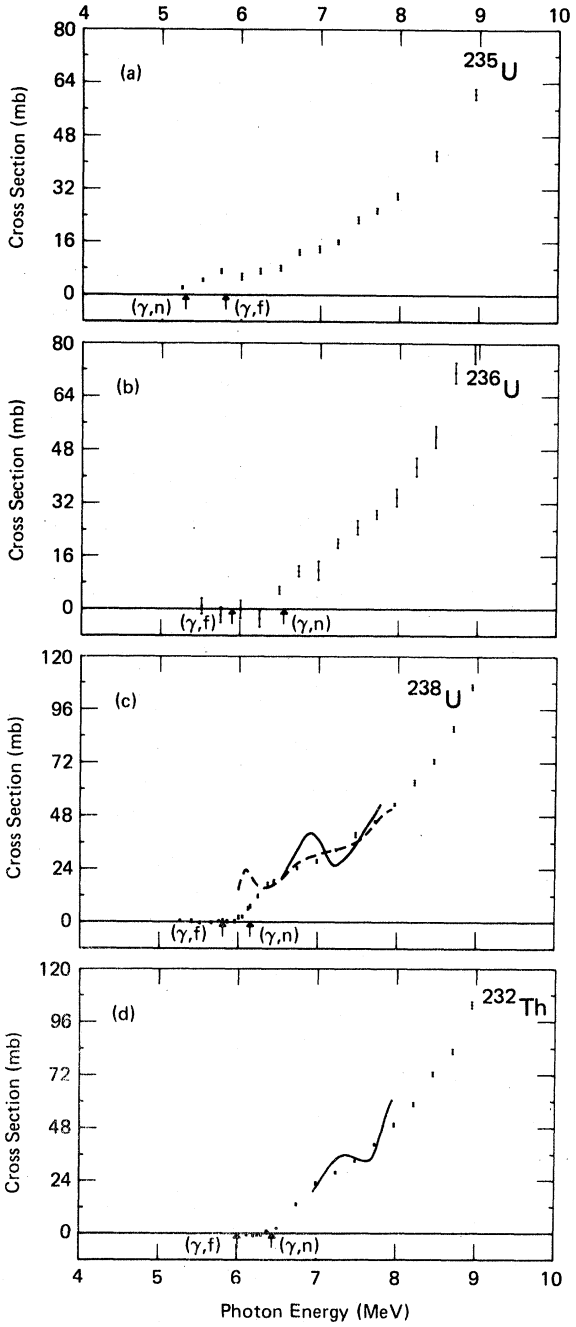

FIG. 11. Low-energy photoneutron cross sections. (a) $\sigma(\gamma,n)$ for ^{235}U: data points—present work; (b) $\sigma(\gamma,n)$ for ^{236}U: data points—present work; (c) $\sigma(\gamma,n)$ for ^{238}U: data points—present work, dashed curve—Chalk River (Ref. 30), solid curve—Illinois (Ref. 33); (d) $\sigma(\gamma,n)$ for ^{232}Th: data points—present work, solid curve—Illinois (Ref. 33).

formed with tagged bremsstrahlung photons, on the other hand, are in better agreement with the present results. These results, from Illinois,[33] are shown as the solid lines in Figs. 10(c) and 10(d). The resolution of these data (~100 keV) is somewhat better than that of the present data, as can be seen in particular from the 6-MeV peak in $\sigma(\gamma, F)$ for ^{238}U.

The low-energy part of the photoneutron cross sections are shown in Fig. 11. The photoneutron cross-section data from Illinois are in fair agreement with the present data for ^{238}U and ^{232}Th [Figs. 11(c) and 11(d)]. The ^{238}U(γ, n) data from Chalk River agree well with the present data above 6.4 MeV [Fig. 11(c)] but their peak at 6.1 MeV does not appear in our data. It might owe its origin to their low value for that peak in $\sigma(\gamma, f)$ [Fig. 10(c)] because they determined $\sigma(\gamma, n)$ by subtracting $\bar{\nu}_p \sigma(\gamma, f)$ from their measured neutron yield cross section $\sigma[(\gamma, n) + \bar{\nu}_p \sigma(\gamma, f)]$ assuming a constant $\bar{\nu}_p$. Our measurement[4] of $\bar{\nu}_p(E_\gamma)$ for ^{238}U in this energy region does not support this assumption. The photoneutron data of Ref. 27 do not agree nearly as well as the others with the present data.

F. Second-chance photofission and nuclear fissionability

The important branching ratio of the neutron-emission width to the fission width, Γ_n/Γ_f, can be determined at low excitation energies directly from $\sigma(\gamma, n)/\sigma(\gamma, F)$ because only first-chance photofission reactions are energetically possible. At higher energies, however, second-chance photofission reactions become possible [the second-chance fission barriers $B_F(\gamma, nf)$ are given in Table I]. One must separate these two components in order to determine Γ_n/Γ_f. One of the virtues of the ring-ratio technique employed in the present experiment (see Sec. III A and Ref. 4) is the ability to decompose $\sigma(\gamma, F)$ into its two components. The ratio of the first-chance photofission cross section $\sigma(\gamma, f)$ to the total photofission cross section $\sigma(\gamma, F) = \sigma[(\gamma, f) + (\gamma, nf)]$ is shown in Figs. 12(a) and 12(b), for ^{236}U and ^{238}U, respectively. [Poor statistics owing to the small size of $\sigma(\gamma, F)$ for ^{232}Th and the relatively large multiplication corrections for ^{235}U make this procedure statistically uncertain for these nuclei.] This decomposition is a new development that might prove to be a significant step in our understanding of the fission process, and it is noteworthy that for both ^{236}U and ^{238}U the first- and second-chance photofission cross sections are approximately equal a few MeV above $B_F(\gamma, nf)$. There also is some indication from the data of Fig. 12 that $B_F(\gamma, nf)$ for ^{238}U might be lower than

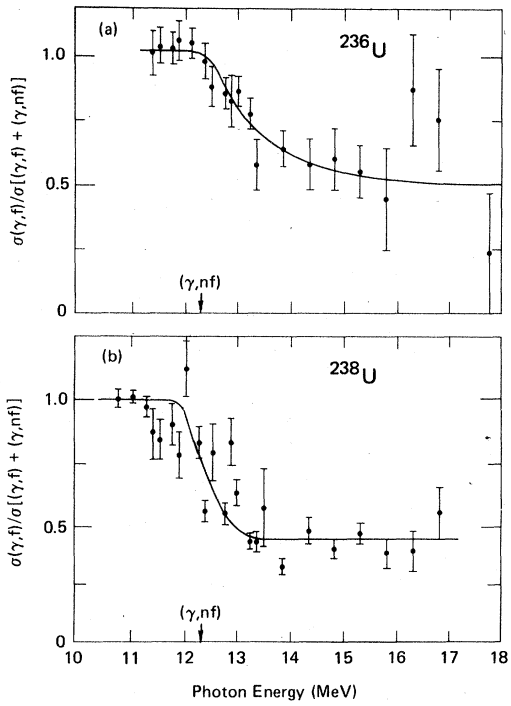

FIG. 12. Ratios of the first-chance photofission cross section $\sigma(\gamma, f)$ to the total photofission cross section $\sigma(\gamma, F) = \sigma[(\gamma, f) + (\gamma, nf)]$: (a) for ^{236}U, (b) for ^{238}U.

the value of 12.3 MeV listed in Table I, which would mean that the value of 6.1 MeV for $B_F(\gamma, f)$ for ^{237}U given in Ref. 9 might be somewhat high.

This decomposition of $\sigma(\gamma, F)$ into $\sigma(\gamma, f)$ and $\sigma(\gamma, nf)$ enables us to determine the total *photoneutron* cross sections $\sigma(\gamma, n_t) = \sigma[(\gamma, n) + (\gamma, 2n) + (\gamma, nf)]$, which in turn enable us to extract Γ_n/Γ_f throughout the energy range studied here. The result of this analysis for the case of ^{236}U is shown in Fig. 13; a similar result is achieved for the case of ^{238}U. Because Γ_n/Γ_f appears to reach an asymptotic value above 9 or 10 MeV, it is therefore reasonable to assume that the same behavior holds for the other nuclei studied; thus, the values for Γ_n/Γ_f determined at 11 MeV should be characteristic of all these nuclei. These values for Γ_n/Γ_f are plotted in Fig. 14 as a function of the nuclear fissionability Z^2/A (see Ref. 9, pp. 16–17 and Ref. 51). Also shown in Fig. 14 are values for Γ_n/Γ_f deduced from the photonuclear data of Veyssière *et al.*[6] and from the charged-particle-induced fission data of Gavron *et al.*[52] The solid symbols in the figure represent values for Γ_n/Γ_f obtained from $\sigma(\gamma, n)/\sigma(\gamma, f)$, while the open symbols for the present data and for those of Ref. 6 represent values for the target-minus-one-neutron nucleus obtained from $\sigma(\gamma, 2n)/\sigma(\gamma, nf)$. [The

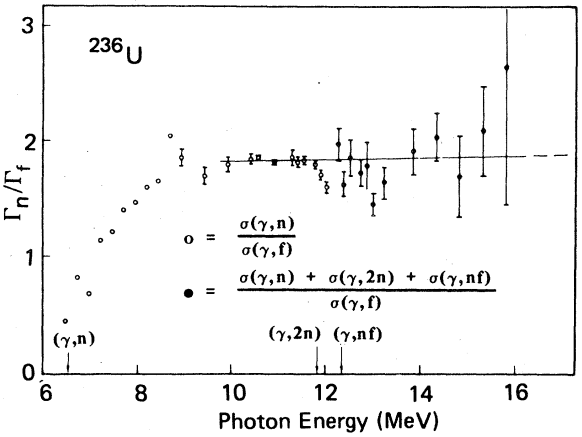

FIG. 13. Neutron-to-fission branching ratio Γ_n/Γ_f versus photon energy for ^{236}U.

values for $\sigma(\gamma, nf)$ used in Ref. 6 were obtained by an extrapolation procedure rather than by a direct determination.] Figure 14 shows the values for Γ_n/Γ_f decreasing exponentially with the fissionability of the nucleus (see the discussion in Sec. III B). Figure 14 also shows that the present

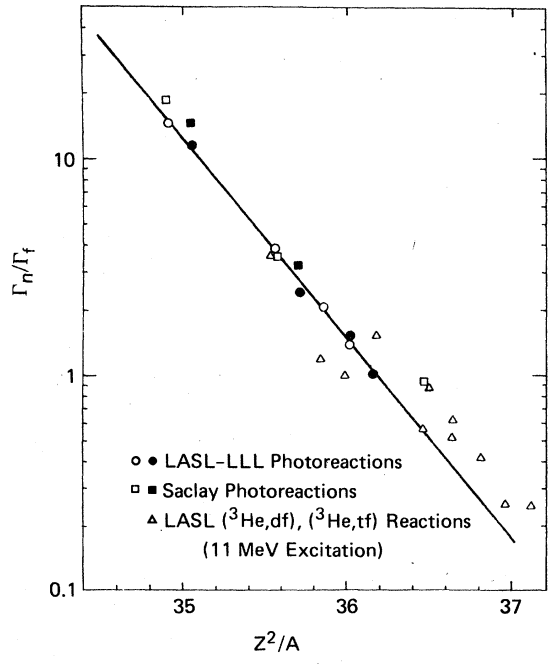

FIG. 14. Neutron-to-fission branching ratio Γ_n/Γ_f at 11-MeV excitation energy versus nuclear fissionability Z^2/A: closed circles—present work, from $\sigma(\gamma,n)/\sigma(\gamma,f)$; open circles—present work, from $\sigma(\gamma,2n)/\sigma(\gamma,nf)$; closed squares—work of Ref. 6, from $\sigma(\gamma,n)/\sigma(\gamma,f)$; open squares—work of Ref. 6 from $\sigma(\gamma,2n)/\sigma(\gamma,nf)$; triangles—work of Ref. 52, from (^{3}He,df) and (^{3}He,tf) reactions.

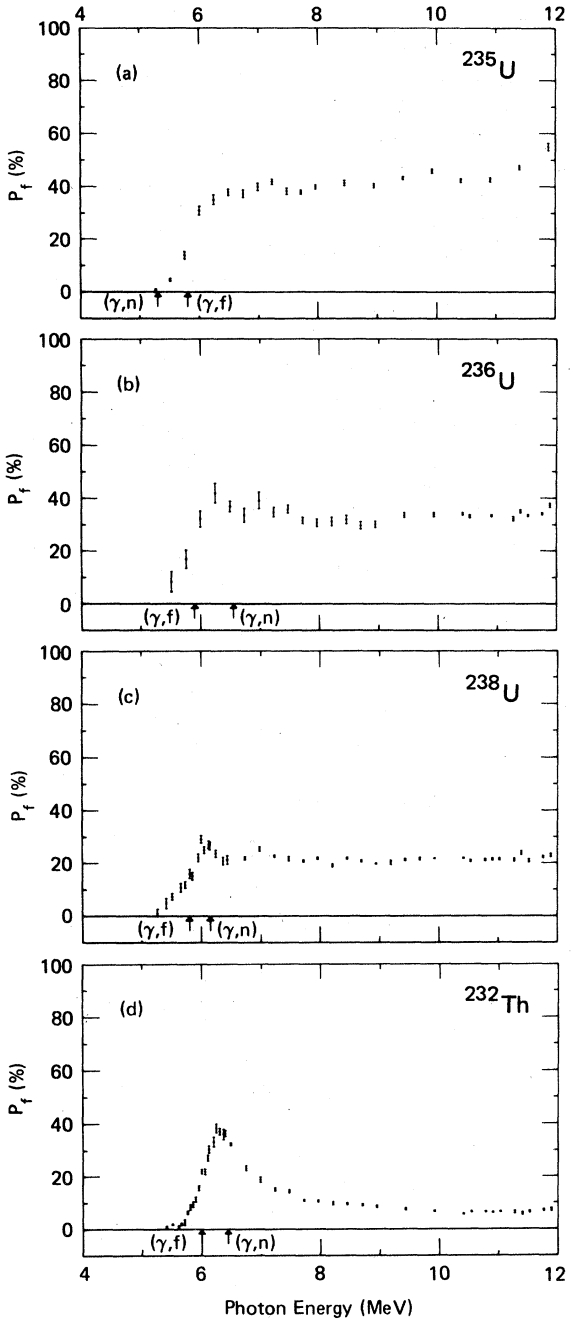

FIG. 15. Fission probability P_f from the ratio of $\sigma(\gamma,f)$ to the value at each energy of the two-component Lorentz-curve fits to the GDR shown in Figs. 2–5: (a) for ^{235}U, (b) for ^{236}U, (c) for ^{238}U, (d) for ^{232}Th.

values for Γ_n/Γ_f from $\sigma(\gamma,n)/\sigma(\gamma,f)$ for ^{235}U and from $\sigma(\gamma,2n)/\sigma(\gamma,nf)$ for ^{236}U are in excellent agreement, thus showing an internal consistency in the experimental data.

Another important nuclear parameter is the

fission probability P_f and its energy dependence. We obtain values for P_f here by dividing the measured (γ,f) cross sections by the values of the two-component Lorentz-curve fits to the GDR obtained in Sec. III C above. This procedure smooths the data in a meaningful way, because the representation of the total photon-absorption cross section by such a curve follows the reasonable (for these nuclei) prescription of the hydrodynamic model. The values for P_f so obtained are shown in Figs. 15(a)–15(d), for ^{235}U, ^{236}U, ^{238}U and ^{232}Th, respectively. The heights of the fission barriers are related closely to the shapes of these P_f-versus-excitation-energy curves, the height of the inner barrier to the shape near threshold, and that of the outer barrier to the asymptotic value.[52] The large decrease in P_f for ^{232}Th above 6.5 MeV [Fig. 15(d)] indicates a sizable component of symmetric fission for this nucleus.[52] The shapes of the P_f curves reported here also can be compared with those resulting from the (t,pf) studies of Britt and collaborators.[53–55] For ^{235}U [Fig. 15(a)], our result is essentially the same as that of Ref. 53. For ^{236}U [Fig. 15(b)], our peak value for P_f (~40%) is much lower than that of Ref. 54 (~80%) but agrees much better with that of the earlier result of Ref. 55 (~50%). Our results for ^{238}U [Fig. 15(c)] are slightly lower than those of Refs. 54 and 55, and are about the same for ^{232}Th [Fig. 15(d)]. Overall, one can say that the agreement both as to magnitude and shape of the present P_f curves with the (t,pf) results is quite good, especially in view of the fact that for photofission the spin of the states excited is limited by the dipole selection rule, whereas no such restriction applies to the (t,pf) reaction. Moreover, a recent analysis[56] for one nucleus (^{238}U) combining the results of both kinds of data suggests that the fission process, at least for that nucleus, is more complex than had been thought previously, and that two distinct second saddle points, one mass asymmetric and the other axially asymmetric, are involved.

IV. SUMMARY

All the major photonuclear cross sections, including those for single- and double-photoneutron emission and for first- and second-chance photofission, have been measured for the four actinide nuclei ^{235}U, ^{236}U, ^{238}U, and ^{232}Th. The magnitudes of all these partial photonuclear cross sections were found to be sensitive functions of the nuclear fissionability (Sec. III B and Figs. 2–5). Their sum is a good approximation to the total photon-absorption cross section and varies little from case to case within the range of nuclei studied here, thus making possible the analysis of the total cross sections by means of the semiclassical hydrodynamic model. Nuclear parameters extracted by this procedure (Sec. III C) include giant-resonance parameters (Table II), nuclear symmetry energies (Table III), and nuclear shape parameters and nuclear radii (Table IV). The integrated cross sections and their moments (Sec. III D, Figs. 6–9, and Tables V and VI) produce no unexpected results when compared with the predictions of various sum rules. Decomposition of total photofission cross sections into their first- and second-chance fission components make possible the determination of the total photo-neutron cross sections and the consequent extraction of the ratio of neutron to fission probabilities (Fig. 13), whose dependence upon fissionability is shown consistently to follow the usual systematic behavior (Fig. 14). Finally, absolute fission probabilities were extracted as well (Fig. 15) and were shown to be in reasonable agreement with corresponding results obtained from (t,pf) measurements.

ACKNOWLEDGMENTS

We thank the operating and mechanical staff of the Lawrence Livermore Laboratory Linac for their expert help. We also thank Dr. T. F. Godlove for his help in the early stages of the experiment. We appreciate the help of Dr. H. F. Atwater who performed the sample multiplication calculations for our work. We also are grateful to Dr. R. Bergère and Dr. B. A. Tulupov for sending us their data in numerical form. Preliminary accounts of part of these data appeared in Refs. 44, 46, and 57; the data presented here supersede those given in all of these earlier reports. This work was performed under the auspices of the U.S. Department of Energy.

[1]A. Bohr, *Proceedings of the International Conference on the Peaceful Uses of Atomic Energy, Geneva, 1955* (United Nations, New York, 1956), Vol. 2, p. 151.

[2]B. L. Berman and S. C. Fultz, Rev. Mod. Phys. 47, 713 (1975).

[3]M. Danos, Nucl. Phys. 5, 23 (1958).

[4]J. T. Caldwell, E. J. Dowdy, R. A. Alvarez, B. L.

Berman, and P. Meyer, Nucl. Sci. Eng. 73, 153 (1980).
[5]C. D Bowman, G. F. Auchampaugh, and S. C. Fultz, Phys. Rev. 133, B676 (1964).
[6]A. Veyssière, H. Beil, R. Bergère, P. Carlos, A. Leprêtre, and K. Kernbach, Nucl. Phys. A199, 45 (1973).
[7]J. R. Huizenga and H. C. Britt, *Proceedings of the International Conference on Photonuclear Reactions and Applications*, edited by B. L. Berman (Lawrence Livermore Laboratory, Livermore 1973), p. 833.
[8]B. S. Bhandari and I. C. Nascimento, Nucl. Sci. Eng. 60, 19 (1976).
[9]R. Vandenbosch and J. R. Huizenga, *Nuclear Fission* (Academic, New York, 1973).
[10]R. O. Haxby, W. E. Shoupp, W. E. Stephens, and W. H. Wells, Phys. Rev. 59, 57 (1941).
[11]B. Arakatsu, Y. Uemura, M. Sonoda, S. Shimizu, and K. Kimura, Proc. Phys. Math. Soc. Jpn. 23, 440 (1941).
[12]G. C. Baldwin and G. S. Klaiber, Phys. Rev. 71, 3 (1947).
[13]R. B. Duffield and J. R. Huizenga, Phys. Rev. 89, 1042 (1953).
[14]J. E. Gindler and J. R. Huizenga, Phys. Rev. 104, 425 (1956).
[15]V. A. Korotkova, P. A. Cherenkov, and I. V. Chuvilo, Dokl. Akad. Nauk SSSR 106, 633 (1956) [Sov. Phys. Dokl. 1, 77 (1956)].
[16]B. I. Gavrilov and L. E. Lazareva, Zh. Eksp. Teor. Fiz. 30, 855 (1956) [Sov. Phys.–JETP 3, 871 (1957)].
[17]L. Katz, K. G. McNeill, M. LeBlanc, and F. Brown, Can. J. Phys. 35, 470 (1957).
[18]L. Katz, A. P. Baerg, and F. Brown, *Proceedings of the Second International Conference on the Peaceful Uses of Atomic Energy* (United Nations, Geneva, 1958), Vol. 15, p. 188.
[19]G. M. Gurevich, L. E. Lazareva, V. M. Mazur, G. V. Solodukhov, and B. A. Tulupov, Nucl. Phys. A273, 326 (1976).
[20]N. S. Rabotnov, G. N. Smirenkin, A. S. Soldatov, L. N. Usachev, S. P. Kapitza, and Yu. M. Tsipenyuk, Yad. Fiz. 11, 508 (1970) [Sov. J. Nucl. Phys. 11, 285 (1970)].
[21]A. V. Ignatyuk, N. S. Rabotnov, G. N. Smirenkin, A. S. Soldatov, and Yu. M. Tsipenyuk, Zh. Eksp. Teor. Fiz. 61, 1284 (1971); [Sov. Phys.—JETP 34, 684 (1972)].
[22]C. D. Bowman, I. G. Schröder, C. E. Dick, and H. E. Jackson, Phys. Rev. C 12, 863 (1975).
[23]V. E. Zhuchko, A. V. Ignatyuk, Yu. B. Ostapenko, G. N. Smirenkin, A. S. Soldatov, and Yu. M. Tsipenyuk, Phys. Lett. 68B, 323 (1977).
[24]L. J. Lindgren, A. Alm, and A. Sandell, Nucl. Phys. A298, 43 (1978).
[25]J. R. Huizenga, K. M. Clarke, J. E. Gindler, and R. Vandenbosch, Nucl. Phys. 34, 439 (1962).
[26]A. Manfredini, L. Fiore, C. Ramorino, H. G. deCarvalho, and W. Wölfli, Nucl. Phys. A127, 637 (1969) and references therein.
[27]O. Y. Mafra, M. F. Cesar, C. Renner, and J. Goldemberg, Nucl. Phys. A236, 1 (1974); O. Y. Mafra, S. Kuniyoshi, and J. Goldemberg, *ibid.* A186, 110 (1972); and references therein.
[28]T. Dragnev, E. Dermendjiev, N. Kalinkova, N. Kashukeev, N. Tschikov, and N. Yaneva, Progress Report on Nuclear Data Activities in Bulgaria, 1973, p. 42.
[29]A. M. Khan and J. W. Knowles, Nucl. Phys. A179, 333 (1972).
[30]J. W. Knowles and O. Y. Mafra, *Proceedings of the International Conference on Photonuclear Reactions and Applications*, edited by B. L. Berman (Lawrence Livermore Laboratory, Livermore, 1973), pp. 647 and 843.
[31]M. V. Yester, R. A. Anderl, and R. C. Morrison, Nucl. Phys. A206, 593 (1973).
[32]R. A. Anderl, M. V. Yester, and R. C. Morrison, Nucl. Phys. A212, 221 (1973).
[33]P. A. Dickey and P. Axel, Phys. Rev. Lett. 35, 501 (1975).
[34]B. L. Berman, J. T. Caldwell, R. R. Harvey, M. A. Kelly, R. L. Bramblett, and S. C. Fultz, Phys. Rev. 162, 1098 (1967).
[35]S. C. Fultz, R. A. Alvarez, B. L. Berman, and P. Meyer, Phys. Rev. C 10, 608 (1974).
[36]J. T. Caldwell and E. J. Dowdy, Nucl. Sci. Eng. 56, 179 (1975).
[37]A. H. Wapstra and K. Bos, At. Data Nucl. Data Tables 19, 215 (1977).
[38]R. L. Bramblett, J. T. Caldwell, B. L. Berman, R. R. Harvey, and S. C. Fultz, Phys. Rev. 148, 1198 (1966).
[39]R. E. Sund, V. V. Verbinski, H. Weber, and L. A. Kull, Phys. Rev. C 2, 1129 (1970).
[40]H. Beil, R. Bergère, P. Carlos, A. Leprêtre, A. Veyssière, and A. Parlag, Nucl. Phys. A172, 426 (1971).
[41]L. M. Young, Ph.D. thesis, University of Illinois, 1972 (unpublished).
[42]J. Terrell, in *Physics and Chemistry of Fission* (IAEA, Vienna, 1965), Vol. II, p. 3; J. Terrell, Phys. Rev. 108, 783 (1957).
[43]J. G. Woodworth, K. G. McNeill, J. W. Jury, R. A. Alvarez, B. L. Berman, D. D. Faul, and P. Meyer, Lawrence Livermore Laboratory Report No. UCRL-77471, 1978.
[44]J. T. Caldwell, E. J. Dowdy, B. L. Berman, R. A. Alvarez, and P. Meyer, Los Alamos Scientific Laboratory Report No. LA-UR 76-1615, 1976.
[45]B. L. Berman, M. A. Kelly, R. L. Bramblett, J. T. Caldwell, H. S. Davis, and S. C. Fultz, Phys. Rev. 185, 1576 (1969).
[46]B. L. Berman, Lawrence Livermore Laboratory Report No. UCRL-78482, 1976.
[47]K. E. G. Löbner, M. Vetter, and V. Hönig, Nucl. Data Tables 7, 495 (1970) and references therein.
[48]A. Migdal, Zh. Eksp. Teor. Fiz. 15, 81 (1945).
[49]J. S. Levinger, *Nuclear Photo-Disintegration* (Oxford University Press, London, 1960), p. 51.
[50]S. C. Fultz, B. L. Berman, J. T. Caldwell, R. L. Bramblett, and M. A. Kelly, Phys. Rev. 186, 1255 (1969).
[51]N. Bohr and J. A. Wheeler, Phys. Rev. 56, 426 (1939).
[52]A. Gavron, H. C. Britt, E. Konecny, J. Weber, and J. B. Wilhelmy, Phys. Rev. C 13, 2374 (1976).
[53]H. C. Britt and J. C. Cramer, Phys. Rev. C 2, 1758 (1970), analyzed in B. B. Back, H. C. Britt, O. Hansen, B. Leroux, and J. D. Garrett, Phys. Rev. C 10, 1948 (1974).
[54]B. B. Back, O. Hansen, H. C. Britt, and J. C. Garrett, Phys. Rev. C 9, 1924 (1974).
[55]J. D. Cramer and H. C. Britt, Phys. Rev. C 2, 2350 (1970).

[56]A. Gavron, H. C. Britt, P. D. Goldstone, J. B. Wilhelmy, and S. E. Larsson, Phys. Rev. Lett. 38, 1457 (1977).
[57]J. T. Caldwell, E. J. Dowdy, R. A. Alvarez, B. L. Berman, P. Meyer, and T. F. Godlove, Bull. Am. Phys. Soc. 20, 582 (1975); J. T. Caldwell, *ibid.* 20, 1187 (1975); B. L. Berman, Lawrence Livermore Laboratory Report No. UCRL-81596, 1978.